Constrained Model Predictive Control for Hybrid Excited Permanent Magnet Synchronous Motors

Luca Cinti*, Ludovico Ortombina*, Petros Karamanakos†, and Nicola Bianchi*.
* University of Padova, Dept. of Industrial Engineering, 35131, Padova, Italy
† Tampere University, Faculty of Information Technology and Communication Sciences, 33100, Tampere, Finland
luca.cinti@studenti.unipd.it, ludovico.ortombina@unipd.it, p.karamanakos@ieee.org, nicola.bianchi@unipd.it

***Abstract*—This paper deals with an indirect model predictive control for hybrid excited permanent magnet motors that controls both the stator and excitation currents. Moreover, to ensure operation within the physical and safety limits of the drive system, the control algorithm accounts for both voltage and current constraints. To this end, the stator current constraint is translated into a voltage constraint that is subsequently linearized by means of the tangent segment closest to the last applied voltage vector. Simulation results show the effectiveness of the proposed control algorithm.**

***Index Terms*—Wound rotor motor, hybrid excited permanent magnet motor, synchronous motor, model predictive control, current constraint.**

I. Introduction

Over the last years, model predictive control (MPC) has gained much popularity both in academia and industry thanks to the increased computational power of microprocessors. MPC has some inherent attractive characteristics compared to conventional control schemes, such as the capability to handle complex multi-input multi-output systems and to account for system constraints [1]–[4]. The inclusion of explicit system constraints ensures the operation of the system at its physical limits without exceeding them [5]. In addition to this, it enables the most favorable system performance as the control action is computed in a coordinated manner since the constraints are accounted for in the optimization process. This feature is in stark contrast to, e.g., the anti wind-up strategy in conventional proportional-integral regulators, where the control action and the physical limitations are performed in separate computational blocks, thus leading to suboptimal performance [6], [7]. Electric drives have two main limits that the controller must deal with, namely, the limited available voltage of the inverter and the maximum motor current that cannot be exceeded.

Electric motor design is affected by the aforementioned system constraints and a trade-off must be found to maximize the dynamic performance and power density. High torque can be achieved by increasing the permanent magnet (PM) flux linkage, but this would lead to a reduced constant power region due to the limited supply voltage [8], [9]. Such a behavior, however, is undesirable in, e.g., new electric motors for traction. Wound rotor (WR) machines are an effective solution for increasing the maximum motor speed but with a lower torque density [10]. Moreover, the efficiency slightly decreases since the rotor flux is completely generated by a dedicated excitation winding. A motor that achieves a favorable trade-off between torque performance, wide constant power region, and high efficiency is the hybrid excited permanent magnet (HEPM) motor. The unique feature of such a motor is a double rotor flux excitation, namely, both PMs and an excitation winding are mounted on the rotor [11], [12]. Tailored control schemes must be developed to exploit this HEPM motor feature, i.e., excitation current policies must be studied [13], [14].

This paper proposes an indirect MPC scheme for HEPM motors that considers both voltage and current constraints such that safe operation of the drive is guaranteed while fully exploiting its potential. The current constraint is formulated as a voltage constraint and it is linearized by employing the tangent segment closest to the last applied voltage vector. In doing so, the proposed method not only ensures the system safety but it is also less computationally demanding compared with conventional ones, making it suitable for an on-chip implementation. The presented simulation results and comparisons with a conventional strategy show the effectiveness of the proposed control scheme.

The paper is organized as follow. In Section II, the HEPM motor model is described whereas the indirect current MPC is presented in Section III. Voltage and current constraint formulations suitable for the MPC problem are derived in Section IV. Finally, the proposed method is assessed in Section V, while conclusions are drawn in Section VI.

II. HEPM Motor Model

The HEPM motor prototype is shown in Fig. 1, and the considered electric drive scheme is depicted in Fig. 2. The voltage equations of an HEPM motor in the rotating reference frame are:

$$\begin{aligned} u_{\mathrm{d}} &= R_{\mathrm{s}} i_{\mathrm{d}} + L_{\mathrm{d}} \frac{\mathrm{d}i_{\mathrm{d}}}{\mathrm{d}t} + M_{\mathrm{e}} \frac{\mathrm{d}i_{\mathrm{e}}}{\mathrm{d}t} - L_{\mathrm{q}} i_{\mathrm{q}} \omega_{\mathrm{me}}, \\ u_{\mathrm{q}} &= R_{\mathrm{s}} i_{\mathrm{q}} + L_{\mathrm{q}} \frac{\mathrm{d}i_{\mathrm{q}}}{\mathrm{d}t} + \omega_{\mathrm{me}} \left(\Lambda_{\mathrm{PM}} + L_{\mathrm{d}} i_{\mathrm{d}} + M_{\mathrm{e}} i_{\mathrm{e}} \right), \\ u_{\mathrm{e}} &= R_{\mathrm{e}} i_{\mathrm{e}} + L_{\mathrm{e}} \frac{\mathrm{d}i_{\mathrm{e}}}{\mathrm{d}t} + \frac{3}{2} M_{\mathrm{e}} \frac{\mathrm{d}i_{\mathrm{d}}}{\mathrm{d}t}, \end{aligned} \tag{1}$$

This study is partially supported by Department of Industrial Engineering, University of Padova, by means of the project SID BIRD224007 and partially carried out within the MOST - Sustainable Mobility Center and received funding from the European Union Next - Generation EU (Piano Nazionale di Ripresa e Resilienza (PNRR) - Missione 4 Componente 2, Investimento 1.4 - D.D. 1022 17/06/2022, CN00000023).

Fig. 1. HEPM motor prototype. The excitation winding can be observed.

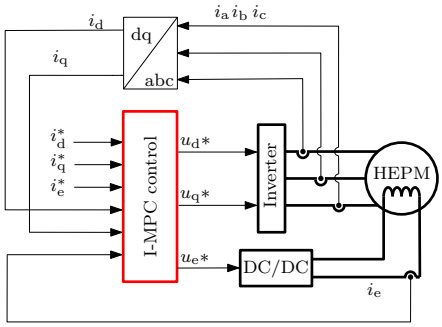

Fig. 2. HEPM motor drive and the proposed control algorithm is highlighted.

where $u_{\mathrm{d,q,e}}$, $i_{\mathrm{d,q,e}}$ and $L_{\mathrm{d,q,e}}$ are respectively the direct, quadrature, excitation voltages, currents and inductances, $R_{\mathrm{s,e}}$ are the stator and excitation resistances, Λ_{PM} is the PM flux linkage, and ω_{me} is the electromechanical speed. Finally, note that the mutual inductance M_{e} is multiplied by 3/2 in the excitation winding voltage equation to take into account the transformation effect. The motor is considered magnetically linear and cross saturation effects are neglected. The motor parameters are reported in Table I.

Reformulating (1) yields:

$$\begin{aligned}
\frac{\mathrm{d}i_{\mathrm{d}}}{\mathrm{d}t} &= \frac{u_{\mathrm{d}} - R_{\mathrm{s}} i_{\mathrm{d}} + L_{\mathrm{q}} i_{\mathrm{q}} \omega_{\mathrm{me}} - \dfrac{M_{\mathrm{e}} u_{\mathrm{e}}}{L_{\mathrm{e}}} + \dfrac{M_{\mathrm{e}} R_{\mathrm{e}} i_{\mathrm{e}}}{L_{\mathrm{e}}}}{L_{\mathrm{d}} - \dfrac{3M_{\mathrm{e}}^2}{2L_{\mathrm{e}}}}, \\
\frac{\mathrm{d}i_{\mathrm{q}}}{\mathrm{d}t} &= \frac{u_{\mathrm{q}} - R_{\mathrm{s}} i_{\mathrm{q}} - \omega_{\mathrm{me}} (\Lambda_{\mathrm{PM}} + L_{\mathrm{d}} i_{\mathrm{d}} + M_{\mathrm{e}} i_{\mathrm{e}})}{L_{\mathrm{q}}}, \\
\frac{\mathrm{d}i_{\mathrm{e}}}{\mathrm{d}t} &= \frac{u_{\mathrm{e}}}{L_{\mathrm{e}}} + \frac{3M_{\mathrm{e}} u_{\mathrm{d}} - R_{\mathrm{s}} i_{\mathrm{d}}}{2(3M_{\mathrm{e}}^2/2 - L_{\mathrm{d}} L_{\mathrm{e}})} + \frac{3M_{\mathrm{e}}^2 u_{\mathrm{e}} - 3M_{\mathrm{e}}^2 R_{\mathrm{e}} i_{\mathrm{e}}}{\sigma_1} + \\
&\quad + \frac{3L_{\mathrm{q}} M_{\mathrm{e}} i_{\mathrm{q}} \omega_{\mathrm{me}}}{2(3M_{\mathrm{e}}^2/2 - L_{\mathrm{d}} L_{\mathrm{e}})} - \frac{R_{\mathrm{e}} i_{\mathrm{e}}}{L_{\mathrm{e}}},
\end{aligned} \tag{2}$$

with $\sigma_1 = 2L_{\mathrm{d}} L_{\mathrm{e}}^2 - 3L_{\mathrm{e}} M_{\mathrm{e}}^2$. Finally, the continuous-time dynamics of the HEPM motor (2) are discretized by using the forward Euler approximation with the sampling interval T_{s} and arranged in the following state-space representation:

$$\begin{aligned}
\mathbf{x}(k+1) &= \mathbf{A}\mathbf{x}(k) + \mathbf{B}\mathbf{u}(k) + \mathbf{D}(k) \\
\mathbf{y}(k) &= \mathbf{C}\mathbf{x}(k)
\end{aligned} \tag{3}$$

where $\mathbf{x} = [i_{\mathrm{d}}, i_{\mathrm{q}}, i_{\mathrm{e}}]^T$ is the state vector, $\mathbf{u} = [u_{\mathrm{d}}, u_{\mathrm{q}}, u_{\mathrm{e}}]$ is the input vector, and $\mathbf{y}$ is the output vector. The matrices $\mathbf{A}$, $\mathbf{B}$, and $\mathbf{D}$ are:

$$\mathbf{A} = \begin{bmatrix}
1 - \dfrac{R_{\mathrm{s}} T_{\mathrm{s}}}{L_{\mathrm{d}} - \dfrac{3M_{\mathrm{e}}^2}{2L_{\mathrm{e}}}} & \dfrac{L_{\mathrm{q}} \omega_{\mathrm{me}} T_{\mathrm{s}}}{L_{\mathrm{d}} - \dfrac{3M_{\mathrm{e}}^2}{2L_{\mathrm{e}}}} & \dfrac{M_{\mathrm{e}} R_{\mathrm{e}} T_{\mathrm{s}}}{L_{\mathrm{d}} L_{\mathrm{e}} - \dfrac{3}{2} M_{\mathrm{e}}^2} \\
-\dfrac{L_{\mathrm{d}} \omega_{\mathrm{me}} T_{\mathrm{s}}}{L_{\mathrm{q}}} & 1 - \dfrac{R_{\mathrm{s}} T_{\mathrm{s}}}{L_{\mathrm{q}}} & -\dfrac{M_{\mathrm{e}} \omega_{\mathrm{me}} T_{\mathrm{s}}}{L_{\mathrm{q}}} \\
-\dfrac{3M_{\mathrm{e}} R_{\mathrm{s}} T_{\mathrm{s}}}{3M_{\mathrm{e}}^2 - 2L_{\mathrm{d}} L_{\mathrm{e}}} & \dfrac{3L_{\mathrm{q}} M_{\mathrm{e}} \omega_{\mathrm{me}} T_{\mathrm{s}}}{3M_{\mathrm{e}}^2 - 2L_{\mathrm{d}} L_{\mathrm{e}}} & \sigma_2
\end{bmatrix},$$

$$\mathbf{B} = \begin{bmatrix}
\dfrac{T_{\mathrm{s}}}{L_{\mathrm{d}} - \dfrac{3M_{\mathrm{e}}^2}{2L_{\mathrm{e}}}} & 0 & -\dfrac{M_{\mathrm{e}} T_{\mathrm{s}}}{L_{\mathrm{e}} \left(L_{\mathrm{d}} - \dfrac{3M_{\mathrm{e}}^2}{2L_{\mathrm{e}}} \right)} \\
0 & \dfrac{T_{\mathrm{s}}}{L_{\mathrm{q}}} & 0 \\
\dfrac{3M_{\mathrm{e}} T_{\mathrm{s}}}{3M_{\mathrm{e}}^2 - 2L_{\mathrm{d}} L_{\mathrm{e}}} & 0 & \dfrac{3M_{\mathrm{e}}^2 T_{\mathrm{s}}}{\sigma_1} + \dfrac{T_{\mathrm{s}}}{L_{\mathrm{e}}}
\end{bmatrix},$$

$$\mathbf{D} = \begin{bmatrix}
0 \\
-\dfrac{\Lambda_{\mathrm{PM}} \omega_{\mathrm{me}} T_{\mathrm{s}}}{L_{\mathrm{q}}} \\
0
\end{bmatrix},$$

where $\sigma_2 = 1 - \dfrac{R_{\mathrm{e}} T_{\mathrm{s}}}{L_{\mathrm{e}}} - \dfrac{3M_{\mathrm{e}}^2 R_{\mathrm{e}} T_{\mathrm{s}}}{\sigma_1}$, while $\mathbf{C} = \mathbf{I}_{3\times3}$, with $\mathbf{I}_{3\times3}$ being the 3×3 identity matrix.

III. MPC Current Control

Indirect MPC (I-MPC) computes the optimal voltage vector $\mathbf{u}_{\mathrm{opt}}(k)$ that is subsequently applied to the power converter by means of a modulator. The controller predicts the system behavior for the next N_{p} steps on the basis of the system model (3) and the applied voltage vector $\mathbf{u}(k-1)$. The optimal voltage input $\mathbf{u}_{\mathrm{opt}}(k)$ is the vector that minimizes a performance index, or cost function, by taking into account system constraints. The chosen cost function is:

$$J(k) = \sum_{l=k}^{k+N_{\mathrm{p}}-1} \|\mathbf{y}^*(l+1) - \mathbf{C}\mathbf{x}(l+1)\|_2^2 + \lambda_u \|\mathbf{u}(l) - \mathbf{u}(l-1)\|_2^2, \tag{4}$$

which quantifies the defined control objectives, namely, the tracking of the stator and excitation current references and the minimization of control input variation. The control priority between the opposing goals is set by the weighting factor λ_u, which defines the trade-off between the tracking ability of the controller and response time during transients. The optimal control input $\mathbf{u}_{\mathrm{opt}}(k)$ is the solution of the following quadratic program (QP):

$$\begin{aligned}
\mathbf{u}_{\mathrm{opt}}(k) = \underset{\mathbf{u} \in \mathbb{R}^3}{\arg\,\mathrm{minimize}}\ & J(k) \\
\text{subject to } & \text{- motor model (3),} \\
& \text{- voltage constraints,} \\
& \text{- current constraints.}
\end{aligned} \tag{5}$$

It is worth noting that for (5) to be a convex QP the current and voltage constraints need to be written as linear inequality

Rated Motor parameter with a DC bus U_{dc} = 300 V					
Mutual inductance	M_{e} = 58 mH	PM flux linkage	Λ_{PM} = 0.6755 V · s	Rated stator current	i_{lim} = 2 A
Rated torque	T_{n} = 5.5 N · m	Excitation current	i_{e} = 2 A	Electrical speed	ω_{me} = 119.38 rad/s
Direct inductance	L_{d} = 157.2 mH	Speed base	n_{N} = 570 rpm	Quadrature inductance	L_{q} = 486.3 mH
Stator resistance (120 °C)	R_{s} = 20.15 Ω	Rotor inductance	L_{e} = 308.4 mH	Rotor resistance	R_{e} = 4.15 Ω

TABLE I. HEPM data motor.

constraints. To this end, a new formulation to include a current constraint is proposed in the sequel.

IV. Voltage and Current Constraints

An inherent MPC feature is the capability to include state and/or input constraints in the optimization problem. Successfully handling such constraints can improve the system performance, in particular when critical operation is desired, e.g., flux-weakening. In electric drives, there are physical constraints that relate to the available voltage provided by the converter and the nominal motor current, which are hereafter described. It is worth remembering that a HEPM motor is characterized by an additional excitation winding, supplied by a dc/dc converter, implying that the relevant constraints must be properly handled.

A. Voltage Constraint

The maximum available voltage for a three-phase two-level inverter can be modeled with a vector that lies in a fixed hexagon in the $\alpha\beta$ reference frame where its size depends on the available dc-bus voltage. Any voltage vector lying within the hexagon can be generated by the converter coupled with a modulator. The hexagon represents the voltage constraint and it can be described by its sides, which in turn can be presented as linear inequality constraints. In doing so, the stator voltage constraints, considering the dq rotating frame, are given by:

$$\begin{bmatrix} \sqrt{3} & 1 & 0 \\ -\sqrt{3} & 1 & 0 \\ 0 & 1 & 0 \\ 0 & -1 & 0 \\ \sqrt{3} & -1 & 0 \\ -\sqrt{3} & -1 & 0 \end{bmatrix} \mathbf{P}^{-1} \begin{bmatrix} u_{\mathrm{d}} \\ u_{\mathrm{q}} \\ u_{\mathrm{e}} \end{bmatrix} \leq \frac{U_{\mathrm{dc}}}{\sqrt{3}} \begin{bmatrix} 2 \\ 2 \\ 1 \\ 1 \\ 2 \\ 2 \end{bmatrix}, \qquad \begin{bmatrix} 0 & 0 & 1 \\ 0 & 0 & -1 \end{bmatrix} \mathbf{P}^{-1} \begin{bmatrix} u_{\mathrm{d}} \\ u_{\mathrm{q}} \\ u_{\mathrm{e}} \end{bmatrix} \leq \begin{bmatrix} u_{\mathrm{e,lim}} \\ u_{\mathrm{e,lim}} \end{bmatrix}, \tag{6}$$

where $\mathbf{P}^{-1}$ is the inverse of the Park transformation and it is reported in Appendix A. Moreover, (6) shows the rotor voltage constraint. Note that the inequality constraints (6) define the "voltage constraints" in the QP (5).

B. Current Constraint

Both the stator and excitation currents must be kept below their nominal values to ensure the safe operation of the motor. To achieve this, additional constraints can be added to the MPC formulation, similarly to the voltage one. By translating the current (i.e., output) constraints into voltage (i.e., input) constraints an ellipsoidal feasible area results in the dq voltage frame. This implies that the current-related voltage constraints are nonlinear, and as such cannot be directly added to the QP (5). Hence, the current constraints must be linearized so that they can be added to the optimization problem. A conventional method suitable for the QP formulation is called linear piecewise method (LPM) [13] and it approximates the nonlinear constraints with a polygon. In doing so, however, the number constraints can increase significantly, making the constrained MPC problem more computationally demanding. In this paper, the equivalent tangent method (ETM) is proposed to mitigate the aforementioned issue. The ETM calculates the tangent line of the nonlinear constraints closest to the last applied voltage vector $\mathbf{u}(k-1)$. As a result, the nonlinear constraints can be approximated with only one linear constraint.

As mentioned above, the stator current constraint is a nonlinear function:

$$i_{\mathrm{d}}(k+1)^2 + i_{\mathrm{q}}(k+1)^2 \leq i_{\mathrm{lim}}^2\,, \tag{7}$$

where i_{lim} is the stator current limit. Expression (7) can be rearranged as a function of the corresponding voltage limits $u_{\mathrm{d,lim}}$ and $u_{\mathrm{q,lim}}$ by exploiting (3), yielding:

$$(c\,u_{\mathrm{d,lim}} + a(k))^2 + (d\,u_{\mathrm{q,lim}} + b(k))^2 \leq i_{\mathrm{lim}}^2\,, \tag{8}$$

where the time-varying coefficients $a(k)$ and $b(k)$, and the constants c and d are:

$$\begin{aligned} a(k) &= i_{\mathrm{d}}(k) - T_{\mathrm{s}} \frac{R_{\mathrm{s}}\, i_{\mathrm{d}}(k)}{L_{\mathrm{d}} - \dfrac{3\,{M_{\mathrm{e}}}^2}{2\,L_{\mathrm{e}}}} + T_{\mathrm{s}} \frac{M_{\mathrm{e}}\, u_{\mathrm{e}}(k) - M_{\mathrm{e}}\, R_{\mathrm{e}}\, i_{\mathrm{e}}(k)}{\dfrac{3\,{M_{\mathrm{e}}}^2}{2} - L_{\mathrm{d}}\, L_{\mathrm{e}}} \\ &\quad + T_{\mathrm{s}} \frac{L_{\mathrm{q}}\, i_{\mathrm{q}}(k)\, \omega_{\mathrm{me}}}{L_{\mathrm{d}} - \dfrac{3\,{M_{\mathrm{e}}}^2}{2\,L_{\mathrm{e}}}}, \\ b(k) &= i_{\mathrm{q}}(k) \left(1 - \frac{R_{\mathrm{s}} T_{\mathrm{s}}}{L_{\mathrm{q}}}\right) + \frac{T_{\mathrm{s}} \omega_{\mathrm{me}}}{L_{\mathrm{q}}} (\Lambda_{\mathrm{PM}} - L_{\mathrm{d}} i_{\mathrm{d}}(k) - M_{\mathrm{e}} i_{\mathrm{e}}(k)), \\ c &= \frac{T_{\mathrm{s}}}{L_{\mathrm{d}} - \dfrac{3\,{M_{\mathrm{e}}}^2}{2\,L_{\mathrm{e}}}}, \qquad d = \frac{T_{\mathrm{s}}}{L_{\mathrm{q}}}. \end{aligned} \tag{9}$$

As can be seen, (8) depicts an ellipsoid in the dq voltage plane, the center and radii of which change according to the operating point. Note that to simplify the mathematical notation, the explicit time-step dependency is omitted hereafter.

1) Linear Piecewise Method: The LPM approximates (8) with n_{a} straight lines, each of which is tangent to the ellipse while all tangency points are equally spaced. According to this

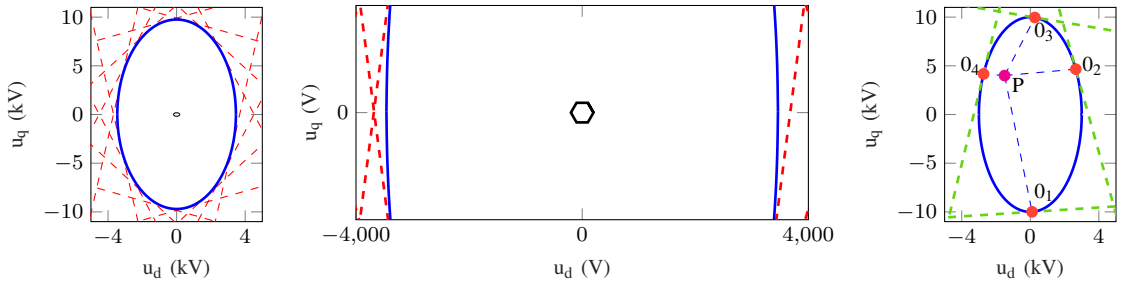

(a) Voltage and current constraints with LPM.

(b) Zoom-in on Fig. 3a.

(c) Voltage and current constraints with ETM.

Fig. 3. Visualization of the LPM and ETM.

method, a generic ellipse (8) can be approximated as follows:

$$\sum_{k=1}^{n_\mathrm{a}} c\,u_\mathrm{d}\cos(k\alpha)+d\,u_\mathrm{q}\sin(k\alpha)\leq i_\mathrm{lim}-a\cos(k\alpha)-b\sin(k\alpha), \tag{10}$$

with the approximation angle $\alpha = 2\pi/n_\mathrm{a}$ and k is a integer number. It is worth noting that the value of n_a can be selected according to the desired level of approximation accuracy. Increasing n_a results in a higher degree of accuracy, but also in a bigger number of summation terms, and thus constraints.

The linearization method (10) can be applied to the voltage constraint (8), yielding the following linear constraints for the QP (5):

$$\mathbf{L}\begin{bmatrix} u_{\mathrm{d,lim}} \\ u_{\mathrm{q,lim}} \\ u_{\mathrm{e,lim}} \end{bmatrix} \leq \mathbf{I}_\mathrm{lim} \tag{11}$$

where

$$\mathbf{L}=\begin{bmatrix} c\cos(\alpha) & d\sin(\alpha) & 0 \\ \vdots & \vdots & \vdots \\ c\cos\Big((n_\mathrm{a}-1)\alpha\Big) & d\sin\Big(n_\mathrm{a}-1)\alpha\Big) & 0 \\ c & 0 & 0 \end{bmatrix}, \tag{12}$$

$$\mathbf{I}_\mathrm{lim}=\begin{bmatrix} i_\mathrm{lim}-a\cos(\alpha)-b\sin(\alpha) \\ \vdots \\ i_\mathrm{lim}-a\cos\Big((n_\mathrm{a}-1)\alpha\Big)-b\sin\Big((n_\mathrm{a}-1)\alpha\Big) \\ i_\mathrm{lim}-a \end{bmatrix}. \tag{13}$$

The linearized constraints with the LPM are reported in Fig. 3a with the actual current-based voltage elliptical constraint. The voltage limit (the hexagon) is depicted as well. The number of approximating lines was set equal to $n_\mathrm{a} = 18$ as trade-off between accuracy and the number of constraints, i.e., complexity of the MPC problem. It is worth noting the different dimension of the voltage and current-based constraints shown in the zoomed-in dq voltage plane in Fig. 3b. Indeed, the former one is more strict.

2) Equivalent Tangent Method: The proposed method exploits the different dimension of the voltage and current-based constraint in the dq reference frame and the fact that only a small part of the ellipsoidal constraint is actually involved in the optimization problem when the current constraint is active. Specifically, the LPM introduces several constraints, most of which are not necessary in the optimization as they set a less restrictive constraint than that imposed by the voltage hexagon. Moreover, the tangent lines are uniformly distributed along the ellipse and, in case of a reduced number of them, the approximation will be very coarse, and thus less effective, meaning that a violation of the actual ellipsoidal constraint becomes more likely.

To overcome this issue, the ETM replaces the ellipse trace with the tangent line closest to the last applied voltage vector. As a result, only one constraint must be included in the QP (5) instead of n_a introduced by the LPM. Fig. 3c illustrates the ETM principle. The point P represents the last applied voltage vector, the ellipse is the current-based constraint and the dashed segments are the four tangent lines orthogonal to the vector $\mathrm{P0_x}$, with $\mathrm{x}\in\{1,2,3,4\}$. The only constraint included in the optimization problem (5) is the tangent line to the point 0_4.

The desired tangent line closest to the last applied voltage vector can be obtained by rewriting the ellipsoidal current constraint (8) in its canonical, i.e.,:

$$\frac{\left(u_{\mathrm{d,lim}}+\dfrac{a}{c}\right)^2}{\left(\dfrac{i_\mathrm{lim}}{c}\right)^2}+\frac{\left(u_{\mathrm{q,lim}}+\dfrac{b}{d}\right)^2}{\left(\dfrac{i_\mathrm{lim}}{d}\right)^2}=1. \tag{14}$$

This expression corresponds to an ellipse centered at $(u_{\mathrm{d,lim}}, u_{\mathrm{q,lim}}) = (a/c, b/d)$. This ellipse can be shifted such that its center is the origin of the dq voltage plane, resulting in:

$$\frac{u_{\mathrm{d,lim}}^2}{\Psi^2}+\frac{u_{\mathrm{q,lim}}^2}{\Theta^2}=1, \tag{15}$$

where $\Psi = i_\mathrm{lim}/c$ and $\Theta = i_\mathrm{lim}/d$. A tangent line to the shifted ellipse (15) at a generic point 0 $(u_{\mathrm{d0}}, u_{\mathrm{q0}})$ can be computed with the help of:

$$\frac{u_{\mathrm{d,lim}}u_{\mathrm{d0}}}{\Psi^2}+\frac{u_{\mathrm{q,lim}}u_{\mathrm{q0}}}{\Theta^2}=1. \tag{16}$$

Finally, (16) can be rewritten in the explicit form as:

$$u_{\mathrm{q,lim}}=\frac{\Theta^2}{u_{\mathrm{q0}}}-\frac{\Theta^2\,u_{\mathrm{d0}}}{\Psi^2\,u_{\mathrm{q0}}}u_{\mathrm{d,lim}}=\ q_\mathrm{r}+m_\mathrm{r}u_{\mathrm{d,lim}}, \tag{17}$$

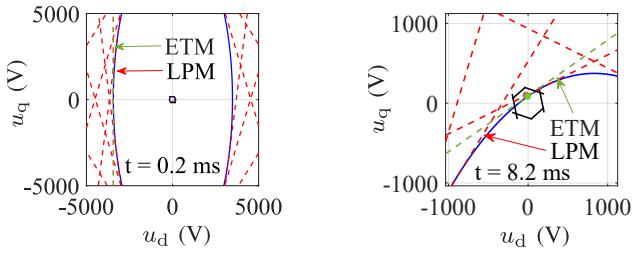

(a) Problem snapshot at 0.2 ms. (b) Problem snapshot at 8.2 ms.

Fig. 4. Voltage and current constraints. Both LPM and ETM are shown.

where m_r and q_r are the angular coefficient and the intercept of the tangent line, respectively.

The angular coefficient of the line segment that connects point P $(u_\mathrm{dP}, u_\mathrm{qP})$ inside the ellipse with point 0 is:

$$m_\mathrm{P0} = \frac{u_\mathrm{qP} - u_\mathrm{q0}}{u_\mathrm{dP} - u_\mathrm{d0}}. \tag{18}$$

With (18), the coordinates of the desired point 0 $(u_\mathrm{d0}, u_\mathrm{q0})$ can be found by solving the following system of equations:

$$\begin{cases} m_\mathrm{r} = -\dfrac{1}{m_\mathrm{P0}} \\ \dfrac{u_\mathrm{d0}^2}{\Psi^2} + \dfrac{u_\mathrm{q0}^2}{\Theta^2} = 1 \end{cases} \Rightarrow \begin{cases} -\dfrac{\Theta^2\, u_\mathrm{d0}}{\Psi^2\, u_\mathrm{q0}} = \dfrac{u_\mathrm{d0} - u_\mathrm{dP}}{u_\mathrm{qP} - u_\mathrm{q0}} \\ \dfrac{u_\mathrm{d0}^2}{\Psi^2} + \dfrac{u_\mathrm{q0}^2}{\Theta^2} = 1 \end{cases} \tag{19}$$

where the first equation imposes the perpendicularity condition between line segment P0 and the tangent lines belonging to the ellipse, while the second equation represents the location of point 0 on the ellipse.

System (19) has four solutions, as depicted in Fig. 3c. Indeed given a point P inside the ellipse, four tangent lines perpendicular to the segment P0 exist. However, the proposed method takes into account only the solution closest to point P. It is worth remembering that the ellipsoidal current constraint has been shifted, meaning that the computed solution must be properly displaced. Hence, Point 0 $(u_\mathrm{d0}, u_\mathrm{q0})$ computed with (19) must be relocated to the original reference system. Given this, the tangent line coefficients in the original dq reference frame can be obtained as follows:

$$\begin{aligned} m'_\mathrm{r} &= m_\mathrm{r}, \\ q'_\mathrm{r} &= \left(u_\mathrm{q0} - \frac{b}{d}\right) - m_\mathrm{r}\left(u_\mathrm{d0} - \frac{b}{d}\right). \end{aligned} \tag{20}$$

With the above, the proposed linearized current constraint tailored for the QP (5) is:

$$\begin{bmatrix} m'_\mathrm{r} & -1 & 0 \end{bmatrix} \begin{bmatrix} u_\mathrm{d,lim} \\ u_\mathrm{q,lim} \\ u_\mathrm{e,lim} \end{bmatrix} < q'_\mathrm{r}, \tag{21}$$

where the coefficients m'_r and q'_r are computed at each discrete time step. Finally, it is worth mentioning that the aforementioned procedure is with regards to the stator currents. Nevertheless, a similar approach can be applied to the excitation current, as reported in Appendix B.

V. Performance Assessment

The proposed ETM was tested by means of simulations. Two different tests were carried out. The first one compares the conventional LPM with the proposed one, whereas the latter examines the capability of the proposed MPC scheme to handle the magnetic mutual coupling between the rotor and stator windings of a HEPM motor. Both tests were carried out at steady-state operating conditions with a speed equal to one third of the nominal one. The stator current references were set equal to $i_\mathrm{d}^* = -0.5\,\mathrm{A}$, $i_\mathrm{q}^* = 1.5\,\mathrm{A}$, whereas the current limits were set equal to $i_\mathrm{lim} = 2\,\mathrm{A}$ and $i_\mathrm{e,lim} = 2.1\,\mathrm{A}$. Other relevant control parameters were $N_\mathrm{p} = 7$, $\lambda_u = 1 \cdot 10^{-3}$ and $n_\mathrm{a} = 18$. The switching frequency was $f_\mathrm{s} = 10\,\mathrm{kHz}$, while the inverter and dc/dc converter voltage buses were set to $U_\mathrm{dc} = 300\,\mathrm{V}$ and $U_\mathrm{dc,\,dc/dc} = 50\,\mathrm{V}$, respectively.

A. Comparison Between LPM and ETM

In this test, the LPM and ETM current constraints are compared while the excitation current reference was set to zero. Fig. 4 shows the dq voltage plane with the voltage and current limits in two different time instants of the test depicted in Fig. 5, namely, when the current limit is not active and when it is activated and thus affecting the optimal solution accordingly. Fig. 4a and Fig. 4b show the dq voltage plane when the current constraint affects the optimal solution, namely, the ellipse intersects the voltage hexagon. All linearized trajectories are depicted as well. The ETM segment better approximates the ellipse, whereas the LPM segments are less accurate. As a result, a violation of the original (i.e. ellipsoidal) current-based constraint is avoided with the proposed method. Moreover, the proposed algorithm keeps the computational burden at bay since only one—instead of n_a—linear constraint is computed.

Fig. 5 shows the current transient and the magnitude of current vector for three different cases, i.e., (a) when only the voltage (hexagon) constraint is used, (b) when the voltage and current-based constraints as approximated with the LPM are used, (c) the same as 'b', but the current-based constraint is approximated with the proposed ETM. In Fig. 5 the voltage constraint is always respected but the current can exceed its limit if the constraint is not included in the optimization problem (see Fig. 5a with $\|\,i\,\|^{\mathrm{vc}}$). On the contrary, the current almost fully respects the defined limit when its constraint is included in (5). However, it is worth noting that the stator current slightly exceeds its maximum allowable value when the LPM is implemented compared to the proposed method, since the linearized ellipse is not accurate enough at the depicted point. The current limitation allows for a smoother transient without affecting the rising time, while the excitation current i_e oscillations are due to the mutual inductances between the stator end excitation windings. Specifically, the HEPM motor exhibits a noteworthy rotor-stator interaction which reflects on currents and torque dynamics. Hence, the motor controller must be able to reject these oscillations as much as possible to improve performance.

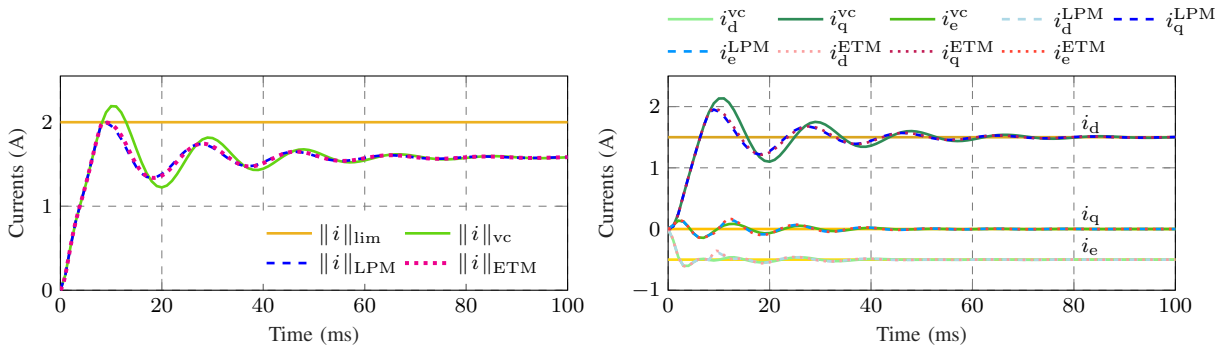

(a) Stator current vector magnitude.

(b) Stator and excitation current response.

Fig. 5. Comparison between voltage (vc) and current constrained MPC solution, both with LPM and the proposed ETM without rotor current.

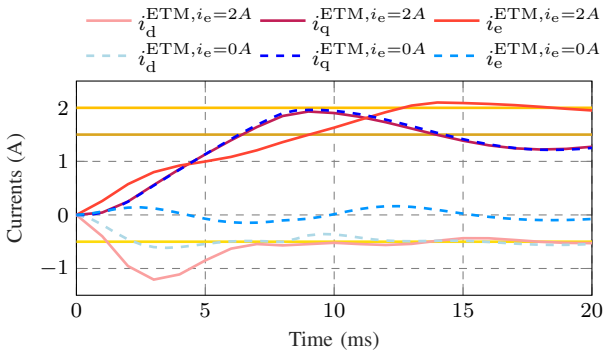

(a) Stator and excitation current response.

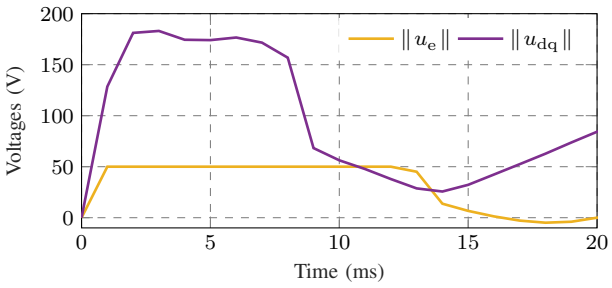

(b) Stator and excitation voltage magnitude.

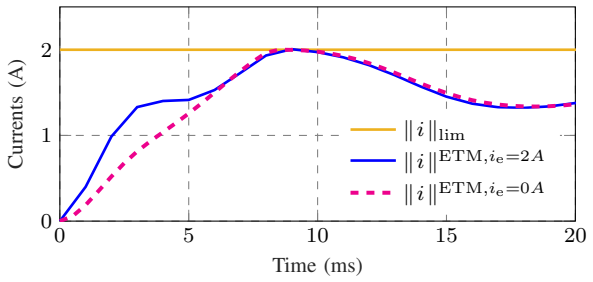

(c) Stator current vector magnitude.

Fig. 6. Dynamic response considering the mutual inductance effect.

B. Mutual Inductance Effect

To analyze the MPC ability to handle the mutual coupling between the stator and rotor windings, an additional test was carried out. More specifically, this test investigates the system behavior when the excitation current reference is zero or close to its limit, namely, $i_{\text{e}}^{*} = 2\,\text{A}$. At the beginning of the test, all currents are initialized to zero and the current constraints are linearized with the proposed ETM. Fig. 6a shows the dynamic behavior of the currents for both considered cases. As can be seen, the quadrature current is not affected by the operating conditions as dictated by the excitation current reference. On the contrary, the direct and excitation currents are strongly coupled, as changes in the excitation current i_{e} have a great impact on the direct current i_{d} amplitude. It is worth noting that the direct current overshoot increases with an increasing excitation current. For the first $3\,\text{ms}$, namely, until the direct current reaches its minimum value, the excitation current increases almost linearly. Indeed, the applied voltage is saturated (see Fig. 6b). After the i_{d} negative peak, and even though the excitation voltage remains saturated, the excitation current i_{e} rate of change decreases since is is affected by the direct current transient. Hence, as MPC tries to track the the direct current reference, it cannot keep the same excitation current slope since the dc/dc voltage is fully exploited. Nevertheless, both the magnitude of the stator current (see Fig. 6c) as well as of the excitation one (see Fig. 6a) remain below the imposed limits, thus clearly demonstrating the effectiveness of the proposed current constraint linearization method.

VI. Conclusion

This paper proposed an indirect MPC control algorithm for HEPM motors. The proposed MPC method is designed based on the HEPM motor model, which, as shown, has intrinsic differences compared with conventional synchronous motors. Moreover, the developed control algorithm accounts for both the voltage and stator and rotor current limits. To achieve this, the nonlinear current constraints are included into the derived QP, after being transformed into equivalent voltage constraints, and linearized by means of the tangent segment closest to the last applied voltage vector. Thanks to this linearization method,

the proposed control scheme is computationally efficient, and thus suitable for an on-chip implementation. Simulation results highlight the efficacy and the reliability of the proposed MPC algorithm as well as the strong coupling between the stator and excitation windings of the HEPM motor.

APPENDIX

A. Inverse Park Transformation

The inverse Park transformation is the following 3×3 matrix:

$$\mathbf{P^{-1}} = \begin{bmatrix} \cos(\omega_{\mathrm{me}}t) & -\sin(\omega_{\mathrm{me}}t) & 0 \\ \sin(\omega_{\mathrm{me}}t) & \cos(\omega_{\mathrm{me}}t) & 0 \\ 0 & 0 & 1 \end{bmatrix}. \tag{22}$$

B. Excitation Current Constraint

The rotor current has to satisfy the current constraint $\| i_{\mathrm{e}}(k+1) \| \leq \| i_{\mathrm{e,lim}} \|$ and it can be written as:

$$\Big(\frac{3\,{M_{\mathrm{e}}}^2}{\sigma_1} + \frac{T_{\mathrm{s}}}{L_{\mathrm{e}}}\Big) u_{\mathrm{e,lim}} + a_{\mathrm{e}}(k) \leq i_{\mathrm{e,lim}}, \tag{23}$$

where:

$$\begin{aligned} a_{\mathrm{e}}(k) = i_{\mathrm{e}}(k) + T_{\mathrm{s}} \Bigg[& \frac{3\,M_{\mathrm{e}}\,u_{\mathrm{d}}(k)}{2\left(\frac{3\,{M_{\mathrm{e}}}^2}{2} - L_{\mathrm{d}}\,L_{\mathrm{e}}\right)} - \frac{R_{\mathrm{e}}\,i_{\mathrm{e}}(k)}{L_{\mathrm{e}}} + \\ & - \frac{3\,M_{\mathrm{e}}\,R_{\mathrm{s}}\,i_{\mathrm{d}}(k)}{2\left(\frac{3\,{M_{\mathrm{e}}}^2}{2} - L_{\mathrm{d}}\,L_{\mathrm{e}}\right)} - \frac{3\,{M_{\mathrm{e}}}^2\,R_{\mathrm{e}}\,i_{\mathrm{e}}(k)}{\sigma_1} + \\ & + \frac{3\,L_{\mathrm{q}}\,M_{\mathrm{e}}\,i_{\mathrm{q}}(k)\,\omega_{\mathrm{me}}}{2\left(\frac{3\,{M_{\mathrm{e}}}^2}{2} - L_{\mathrm{d}}\,L_{\mathrm{e}}\right)} \Bigg]. \end{aligned} \tag{24}$$

The rotor current constraint can be written for both positive and negative values as:

$$\begin{bmatrix} 0 & 0 & \frac{3T_{\mathrm{s}}\,{M_{\mathrm{e}}}^2}{\sigma_1} + \frac{T_{\mathrm{s}}}{L_{\mathrm{e}}} \\ 0 & 0 & -\frac{3T_{\mathrm{s}}\,{M_{\mathrm{e}}}^2}{\sigma_1} - \frac{T_{\mathrm{s}}}{L_{\mathrm{e}}} \end{bmatrix} \begin{bmatrix} u_{\mathrm{d,lim}} \\ u_{\mathrm{q,lim}} \\ u_{\mathrm{e,lim}} \end{bmatrix} \leq \begin{bmatrix} i_{\mathrm{e,lim}} - a_{\mathrm{e}}(k) \\ i_{\mathrm{e,lim}} - a_{\mathrm{e}}(k) \end{bmatrix}, \tag{25}$$

and can be included in the QP (5). It is worth noting that only one of the two constraints needs to be used in order to reduce the size of the optimization problem. Specifically, if the current reference is positive, the upper limit is used, otherwise the lower one.

REFERENCES

[1] S. Vazquez, J. Rodriguez, M. Rivera, L. G. Franquelo, and M. Norambuena, "Model predictive control for power converters and drives: Advances and trends," *IEEE Trans. on Ind. Electron.*, vol. 64, no. 2, pp. 935–947, 2017.

[2] P. Karamanakos, E. Liegmann, T. Geyer, and R. Kennel, "Model predictive control of power electronic systems: Methods, results, and challenges," *IEEE Open J. of Ind. Appl.*, vol. 1, pp. 95–114, 2020.

[3] G. Cimini, D. Bernardini, S. Levijoki, and A. Bemporad, "Embedded model predictive control with certified real-time optimization for synchronous motors," *IEEE Trans. on Control Syst. Technol.*, vol. 29, no. 2, pp. 893–900, 2021.

[4] M. Rossi, P. Karamanakos, and F. Castelli-Dezza, "An indirect model predictive control method for grid-connected three-level neutral point clamped converters with LCL filters," *IEEE Trans. on Ind. Appl.*, vol. 58, no. 3, pp. 3750–3768, May/Jun. 2022.

[5] A. Favato, P. G. Carlet, F. Toso, R. Torchio, L. Ortombina, M. Bruschetta, R. Carli, P. Alotto, S. Bolognani, and J. Rodriguez, "Fast solver for implicit continuous set model predictive control of electric drives," *IEEE Access*, vol. 10, pp. 17 430–17 440, 2022.

[6] N. Bottrell and T. C. Green, "Comparison of current-limiting strategies during fault ride-through of inverters to prevent latch-up and wind-up," *IEEE Trans. on Power Electron.*, vol. 29, no. 7, pp. 3786–3797, 2014.

[7] M. N. Hussain, G. Melath, and V. Agarwal, "An active damping technique for pi and predictive controllers of an interlinking converter in an islanded hybrid microgrid," *IEEE Trans. on Power Electron.*, vol. 36, no. 5, pp. 5521–5529, 2021.

[8] G. Pellegrino, A. Vagati, B. Boazzo, and P. Guglielmi, "Comparison of induction and pm synchronous motor drives for ev application including design examples," *IEEE Trans. on Ind. Appl.*, vol. 48, no. 6, pp. 2322–2332, 2012.

[9] Y. Xiao, Z. Q. Zhu, G. W. Jewell, J. T. Chen, D. Wu, and L. M. Gong, "A novel asymmetric interior permanent magnet synchronous machine," *IEEE Trans. on Ind. Appl.*, vol. 58, no. 3, pp. 3370–3382, 2022.

[10] J. Tang and Y. Liu, "Design of electrically excited synchronous machines to achieve unity power factor in field weakening for long-haul electric trucks," in *2020 Int. Conf. on Elect. Mach. (ICEM)*, vol. 1, 2020, pp. 422–428.

[11] U. K. Mudhigollam, U. Choudhury, and K. Hatua, "A new rotor excitation topology for hybrid excitation machine," in *2016 IEEE Int. Conf. on Power Elec., Drives and Energy Syst. (PEDES)*, 2016, pp. 1–6.

[12] Y. Amara, S. Hlioui, H. B. Ahmed, and M. Gabsi, "Power capability of hybrid excited synchronous motors in variable speed drives applications," *IEEE Trans. on Magn.*, vol. 55, no. 8, pp. 1–12, 2019.

[13] S. Mariethoz, A. Domahidi, and M. Morari, "High-bandwidth explicit model predictive control of electrical drives," *IEEE Trans. on Ind. Appl.*, vol. 48, no. 6, pp. 1980–1992, 2012.

[14] L. Kefsi, Y. Touzani, and M. Gabsi, "Hybrid excitation synchronous motor control with a new flux weakening strategy," in *2010 IEEE Vehicle Power and Propul. Conf.*, 2010, pp. 1–5.

Luca Cinti received the M.S degrees in electrical engineering from the University of Padova, Padova, Italy, in 2020. He is currently working toward the Ph.D. degree in electrical engineering with the Department of Industrial Engineering, University of Padova. His research interests include the design of hybrid, wound excited synchronous machines and their electrical drives.

Ludovico Ortombina (Member, IEEE) received the M.S. and Ph.D. degrees in mechatronics engineering from the University of Padova, Italy, in 2015 and 2019, respectively. Since August 2020, he has been a Researcher with the Department of Industrial Engineering, University of Padova. His research interests include parameter estimation techniques for synchronous motors, sensorless controls, and predictive control.

Petros Karamanakos (Senior Member, IEEE) received the Diploma and the Ph.D. degrees in electrical and computer engineering from the National Technical University of Athens, Greece, in 2007, and 2013, respectively. Since 2016, he has been with the Faculty of Information Technology and Communication Sciences, Tampere University, Finland, where he is currently an Associate Professor. Prior to joining the Tampere University, he was with the ABB Corporate Research Center, Switzerland, and the Chair of Electrical Drive Systems and Power Electronics, Technische Universität München, Germany. His research interests lie at the intersection of optimal control, mathematical programming, and power electronics.

Nicola Bianchi (Fellow, IEEE), is a Full Professor of electrical machines, converters, and drives at Electric Drive Laboratory, Department of Electrical Engineering, University of Padova. His research deals with design and control of electrical machines. He is author of several scientific papers and international books on electrical machines and drives, and he is a recipient of nine awards for best conference and journal papers.